2023

Chemometrics and Spectroscopic Analyses of Peganum harmala Plant's Seeds by Laser-Induced Breakdown Spectroscopy

Tahani A. Alrebdi
Princess Nourah bint Abdulrahman University

Amir Fayyaz
Quaid-i-Azam University Campus

Haroon Asghar
Quaid-i-Azam University Campus

Asif Kamal
Quaid-i-Azam University

Javed Iqbal
University of Azad Jammu & Kashmir

See next page for additional authors

Recommended Citation

Authors

Tahani A. Alrebdi, Amir Fayyaz, Haroon Asghar, Asif Kamal, Javed Iqbal, and Naveed K. Piracha

Article

Chemometrics and Spectroscopic Analyses of *Peganum harmala* Plant's Seeds by Laser-Induced Breakdown Spectroscopy

Tahani A. Alrebdi [1,†], Amir Fayyaz [2,†], Haroon Asghar [2,*], Asif Kamal [3], Javed Iqbal [4] and Naveed K. Piracha [5]

[1] Department of Physics, College of Science, Princess Nourah bint Abdulrahman University, P.O. Box 84428, Riyadh 11671, Saudi Arabia

[2] National Centre for Physics, Quaid-i-Azam University Campus, Islamabad 45320, Pakistan

[3] Department of Plant Sciences, Faculty of Biological Sciences, Quaid-i-Azam University, Islamabad 45320, Pakistan

[4] Department of Physics, King Abdullah Campus, University of Azad Jammu & Kashmir, Muzaffarabad 13100, Pakistan

[5] Department of Physics, John Carroll University, University Heights, OH 44118, USA

* Correspondence: haroon.asghar92@gmail.com

† These authors contributed equally to this work.

Abstract: In the present work, the rapid identification of elements and their relative chemical composition in various *Peganum harmala* seed samples were investigated using a calibration-free laser-induced breakdown spectroscopy technique (CF-LIBS). A pulsed Nd:YAG laser-source with a 5 ns pulse-duration, and 10 Hz pulse repetition rates providing 400 and 200 mJ energy at 1064 and 532 nm wavelength, respectively, was focused on the *Peganum harmala* seed samples for ablation. A LIBS 2000+ spectrometer within the wavelength range (200 to 720 nm), emission-spectra were recorded. The measured spectra of the *Peganum harmala* sample gives spectral lines of Carbon (C), Magnesium (Mg), Lithium (Li), Sodium (Na), Calcium (Ca), Silicon (Si), Iron (Fe), Strontium (Sr), Copper (Cu), Potassium (K), and Lead (Pb). A CF-LIBS technique has been employed for the compositional study of the elements exist in the *Peganum harmala* seed samples. The measured results demonstrate that C, Mg, and Ca are found to be major elements in the *Peganum harmala* seed samples with compositions of ~36.64%, ~24.09%, and ~19.03%, respectively. Along with the major elements, the elements including Li, Na, Si, K, Fe, and Sr were identified as minor elements with compositions of ~2.87%, ~2.33%, ~3.72%, ~7.17%, ~2.83%, and ~1.14%, respectively. Besides Cu (~8.07 μg/g), and Pb (~1.10 μg/g) elements were observed as trace elements exist in the *Peganum harmala* seed samples. Furthermore, the electron number density including the plasma excitation-temperature were calculated using the stark-broadening line profile method and the Saha–Boltzmann plot method, respectively. The plasma parameters versus laser-irradiance and the distance from the sample were further investigated. Moreover, a principal component analysis (PCA) method was also utilized to the spectral data obtained by using LIBS to discriminate various seed samples with four classes, namely, α, β, γ, and Δ. Three principal-components (PCs) calculated from eigenvalues of score matrix described 87.6%, 4.6%, and 2.5% of total variance for PC1, PC2, and PC3, respectively. The LIBS spectral data variance covered by the initial 3 PCS was found as ~94.7% of total variance. The PCA results have successfully demonstrated the different classes of the *Peganum harmala* seed samples based on the different doping compositional ratios of the Zn element. This study confirmed the feasibility and ability of LIBS and PCA for the rapid analysis of *Peganum harmala* seed samples. Finally, the results achieved using CF-LIBS were incorporated with those obtained from the XRF and EDX analytical techniques.

Keywords: *Peganum harmala;* CF-LIBS; quantitative analysis; plasma parameters; PCA; EDX and XRF

1. Introduction

Peganum harmala (*P. harmala*) is generally famous as a Wild-rue flowering plant and is majorly found in North Africa, Middle East, and Asia. The species of *Peganum* are mostly distributed in the Middle East, the Mediterranean, India, Pakistan, Turkey, North Africa, and Iran [1]. *P. harmala* is an ornamental plant with many-branched stems having a white flowering plant [2]. *P. harmala* is used in different eras in different forms. Asian people burn the seeds of *P. harmala* to produce smoke against voodoo [3]. For many years, it has been utilized as a traditional-medicine for the cure of different disorders, like lumbago, jaundice, colic, and asthma [4]. In recent pharmaceutical research, additional medicinal uses of this plant have been explored such as insecticidal properties, anti-cancer properties, anti-malarial [5], anti-parasitic [6], and anti-spasmodic properties [7], as well as anti-oxidant potential, wound curative, immune booster [8], anti-diabetic properties [9], anti-inflammatory effect, and analgesic [10]. It is also documented that *P. harmala* has antifungal, antibacterial, and antiviral potential [11]. The fruits of this plant are used as the source of oil and red dye [12]. The universally called phytochemical-compounds isolated from *P. harmala* are alkaloids, terpenoids, flavonoids, anthraquinones, and steroids [12]. The total phytochemical content of *P. harmala* is different in various plant parts [13]. Harmaline is the major alkaloid that was first time extracted from the roots and seeds of *P. harmala*. Similarly, quinazoline, vaccine, and vasicinone were first isolated in the stems and flowers of this plant [14]. Besides these phytochemicals, the various elements including metals and non-metals have been identified using instrumental neutron activation analysis [15]. Hence, due to their potential applications of *P. harmala* in pharmaceutical industries, a quantitative and discrimination analysis of the trace, minor, and major element ingredients in *P. harmala* is necessary to monitor the pharmacological activities of *P. harmala* seeds.

Laser-induced breakdown spectroscopy (LIBS) has been established to be a quick and negligibly damaging tool for an almost entire compositional analysis of numerous ingredients with tiny or no-sample preparation compared with conventionally available spectroscopic techniques [16–19]. LIBS has potential applications in various fields including industry, deep-sea study, environmental checking, explosives investigation, agriculture, food, and biomedicine [20–29]. LIBS technique yields emission spectra of the sample under investigation which consist of distinctive spectral lines belongs to the various elements present in the target material including gases, liquids, and solids [30–33]. As, individual spectral line in the emission spectra belongs to a unique element present in the periodic table; therefore, LIBS-technique could be utilized for the quantitative investigations of the sample. However, the accurate determination of quantitative analysis in a given sample is not straightforward; the main challenges are self-absorption, matrix effects, and spatial-inhomogeneity [34,35]. These challenges have strong influence on the quality and accuracy of results measured using CF-LIBS. From an experimental view point, the best convenient method to achieve quantitative LIBS analysis depend on formation of calibration-curves utilizing matrix-matched-standards. On the other side, in everyday circumstances, available reference samples are frequently inaccessible or limited. CF-LIBS is a complementary technique built on plasma characterization for achieving compositional analysis without calibrated samples. Reasonable calculations have been achieved with CF-LIBS in soil, cement, sand, plant biochar, geological, and mineralogical samples. Singh et al. [9], Mahmoudian et al. [14], and Anjum et al. [15] evaluated the toxicity, elemental characterization, and anti-diabetic and anti-oxidative effects using *P. harmala* samples. Besides, only a few number of studies have been reported in the appropriate literature belongs to the chemical compositional analysis of elements in *P. harmala* seed samples.

In contrast, chemometrics associated with LIBS has become another interesting topic, which is used to extract important information by reducing the noise data from the acquired LIBS spectra. In particular, chemometrics studies like principal component analysis (PCA) improves the detection accuracy as well as reduces the detection limit [36,37].

In our more recent work [38], we used PCA to distinguish various plant biochar samples based on optically thin emission lines from the laser-produced plasma.

The present work aimed to estimate significance of chemometrics-assisted LIBS for compositional, quantitative, and discrimination analysis of *P. harmala* seed samples. For this purpose, a set of *P. harmala* seeds raw and calibrated samples were investigated along with the study of CN-diatomic molecular emission from the violet system. For the elemental study, LIBS results were compared with those obtained from EDX and XRF analytical techniques showing excellent detection significance of the LIBS measurements. To the best of our knowledge, this is the first study of *P. harmala* seed samples using LIBS-assisted chemometrics analysis. The information from this study will be valuable to monitor the quality of the medicines based on the *P. harmala* seed samples.

2. Experimental Setup and Methods

For LIBS analysis, the laser source which we used in this experimental arrangement is a Nd: YAG laser source ((Quantel-Brilliant-B), France) second-harmonic (2ω), having a repetition-frequency of 10 Hz, 532 nm optical-wavelength, pulse-duration of 5 ns, and provides pulse energy around 200 mJ [38,39]. The experimental arrangements of the LIBS setup were conducted at room-temperature. The laser produces a beam which was focused onto the target surface using a convex-lens (quartz) having a 20 cm focal-length. The target samples were kept on a rotating-stage to provide a fresh sample surface for each laser pulse shot. An optical-emission-spectra were captured through an optical-fiber connected to a charge-coupled devices (CCDs) array spectrometer having a wavelength range varies from 200 to 720 nm [40,41]. Besides the target sample was cleaned with the help of an average of five to seven laser shots on the sample surface.

For EDX measurement, an Oxford-Instruments X-MAX-N-20 EDX-instrument in combination with a scanning-electron-microscope (SEM) machine capable of running at ~30 keV threshold energy was used to estimate chemical-composition of all the seed samples. Similarly, an X-ray fluorescence JSX-3202-M system functioned at 5 to 50 kV varies from 0.01-1.0 mA with a high optical resolution of 150 eV at 6.0 keV was used in this study for the measurement of elemental analysis of seed samples.

Table 1 summarizes the chemical composition (μg/g) of zinc in various *P. harmala* seed samples along with the standard deviation (SD) within the same sample. To study the samples by LIBS, the samples were cleaned in an ultrasonic-bath by wetting them for 50 mins in acetone. Furthermore, the sample was dried for 80 min at 100 °C in an oven to remove moisture. It was then finely ground to achieve homogeneity. The pellet of about 10-mm in diameter as well as 5 mm thick was prepared as a raw sample by exerting about 7 tons of pressure. For the discrimination analysis, several samples (α, β, γ, and δ) were prepared by adding different compositions (μg/g) of zinc in the as-prepared raw powder of *P. harmala* seeds.

Table 1. Prepared standard samples of P. harmala seeds using zinc as dopant material in μg/g.

Element	Sample-(α) (1)	Sample-(β) (3)	Sample-(γ) (3)	Sample-(δ) (3)
Zinc (Zn) [μg/g]	0	45–55	60–65	70–80
Mean ± SD	0	50 ± 2.31	62.5 ± 1.19	75 ± 3.15

3. Results

3.1. Optical Emission Spectra Studies

An emission spectrum of all the *P. harmala* seed samples including raw and as-prepared standard samples were recorded at a fixed laser-pulse-energy of 80 mJ. The measured optical-emission-spectrum from laser-produced plasma was obtained with a CCDs array-spectrometer covers the wavelength range varies from 200 to 720 nm. The spectrum was then further studied by identifying the spectral-lines using NIST Database. The emission spectra of *P. harmala* raw seed sample is given within the wavelength range from 245 nm to 700 nm in Figure 1. The spectral transitions belong to the different elements have various line-intensities which were detected in the raw seed sample.
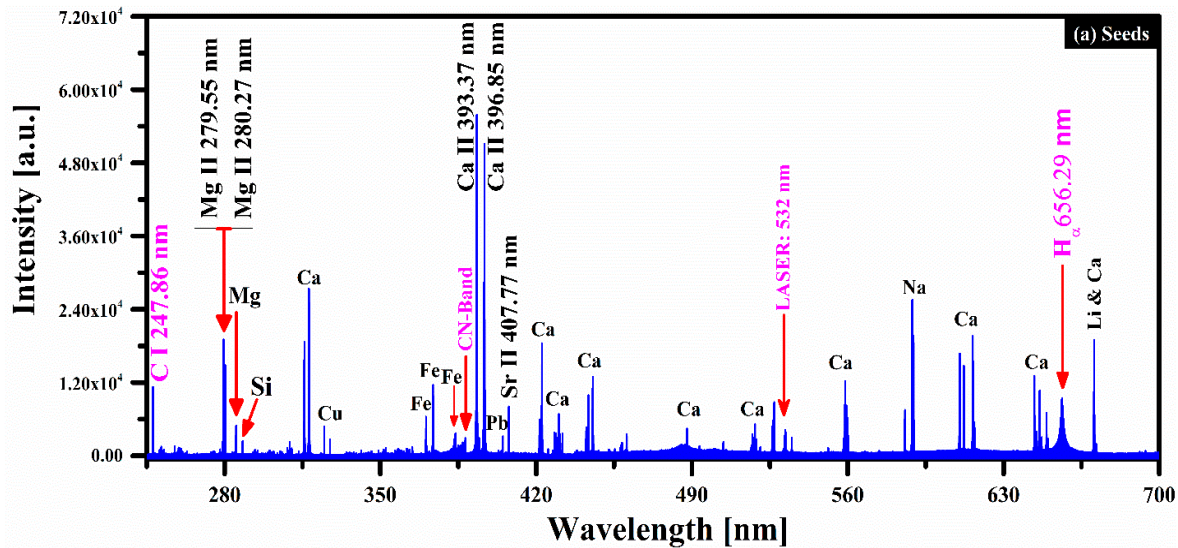

Figure 1. The spectrum of the *P. harmala* seed sample-(α) within the wavelength ranges from 245 nm to 700 nm.

The optical spectrum indicates weak and strong emission lines of different elements including hydrogen (H), lead (Pb), calcium (Ca), carbon (C), lithium (Li), strontium (Sr), silicon (Si), sodium (Na), iron (Fe), and copper (Cu) along with singly ionized magnesium (Mg II) belongs to the 3d $^2D_{3/2,5/2} \to$ 3p $^2P_{1/2,3/2}$ and 3p $^2P_{1/2,3/2} \to$ 3s $^2S_{1/2}$ transitions. In addition, a carbon–nitrogen (CN)-diatomic molecular emission band around 388 nm is detected showing the carbon presence in the seed sample.

In Figure 2, the optical emission-spectrum of the *P. harmala* standard doped seed sample-(δ) is shown at the same optimized LIBS parameters covers wavelength ranges from 240 to 700 nm. The spectral transitions of different elements having diverse line-intensities were noticed in this spectrum of standard doped seed sample-(δ). The optical spectrum of the sample-(δ) shows the atomic and ionic-emission-lines of different elements including H, Mg II, Cu, Pb, Si, Sr, C, Fe, Ca, Na, and Li. The emission line of Zn I having a good signal-to-noise ratio (SNR) in this spectral range, appears at 307.59, 328.23, 330.28, 334.53, 468.01, 472.22, 481.05, 280.12, and 636.23 nm, due to $4s4p\ ^3P_1 \to 4s^2\ ^1S_0$, $4s4d\ ^3D_1 \to 4s4p\ ^3P_0$, $4d\ ^3D_1 \to 4p\ ^3P_1$, $4d\ ^3D_3 \to 4p\ ^3P_2$, $5s\ ^3S_1 \to 4p\ ^3P_0$, $5s\ ^3S_1 \to 4p\ ^3P_1$, $5s\ ^3S_1 \to 4p\ ^3P_2$, $5d\ ^3D_1 \to 4p\ ^3P_2$, $4d\ ^1D_2 \to 4p\ ^1P_1$ transitions, respectively. A single ionic emission line of zinc (Zn II) is also identified at 255.79 nm due to the $5s\ ^2S_{1/2} \to 4p\ ^2P_{3/2}$ transition. Besides, it is pertinent to mention here that various neutral as well as singly ionized emission lines of Ca at optical wavelengths 315.89, 317.93, 393.37, 396.85, 442.54, 443.50, 445.48, 527.03, 558.20, 558.88, 559.01, 559.45, 559.85, 612.22, 616.13, and 616.2 nm are identified with significantly

strong spectral-line-intensities with a good concentration of Ca in seed samples. Moreover, CN-diatomic molecular emission bands around 388 nm are also detected in the doped seed sample-(δ) due to the vibrational transitions.
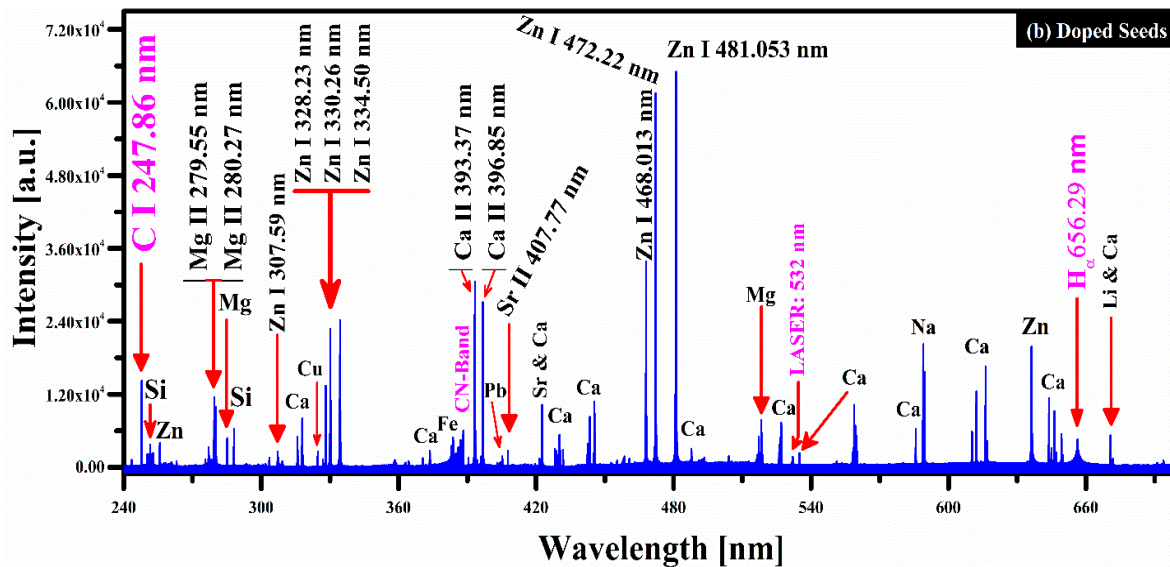

Figure 2. The emission spectrum of the doped P. harmala seed sample-(δ) within the wavelength varies from 240 nm to 700 nm.

In addition, CN-diatomic molecular emissions can also be analyzed in a LIBS spectrum. It has been studied for several descriptions such as plasma characterizations [42], normalization of line-intensities [43], and analysis of organic materials [44]. The CN violet-system ($B^2\Sigma^+$–$X^2\Sigma^+$) with $\Delta v = 0$ has already been studied as a molecular signature for organic compounds [45]. However, CN-bands are essentially unexplored, especially in various medicinal plants for qualitative analysis. In Figures 1 and 2, the observed CN-diatomic molecular bands are associated to (0,0), (1,1), (2,2), (3,3), and (4,4) vibrational transitions at optical wavelength 388.34, 387.14, 386.19, 385.47, and 385.09 nm, respectively. Moreover, atomic emission lines of iron (Fe) at wavelength 383.33 nm and 383.93 nm are identified due to $3d^7(^4P)4p\ ^5D_4 \rightarrow 3d^64s^2\ ^3F_4$ and $3d^6(^3F_2)4s4p(3P)\ ^1G_4 \rightarrow 3d^7(^2G)4s\ ^1G_4$ transitions, respectively. The observed CN-diatomic emissions in the plasma of doped sample-(δ) and undoped sample-(α) are showing strong intensities. The spectral CN line profiles associated with a plasma of doped and undoped *P. harmala* seed samples are comparable to previous reports [46].

3.2. Plasma Excitation Temperature

The excitation-temperature is a significant plasma parameter that could be measured using the Saha–Boltzmann-plot-method including Boltzmann-plot-method. In the Boltzmann plot approach, only the atomic emission spectral lines are essential while in the Saha–Boltzmann plot technique, numerous spectral emission lines such as ionic as well as atomic lines of the corresponding elements are required. To plot both species such as atomic and ionic on the same Boltzmann-type plot, Equation (1) can be utilized. To place both species (ions and neutrals) on the similar plot, the change in abscissas and ordinates of ion points is desired. We adjust the abscissa a measurements of the ionic energy-levels ($E_J^{z^*}$) only by inserting modified ionization energy such as $E_J^{z^*} = E_J^z + \sum_{k=0}^{z-1}(E_\infty^k - \Delta E_\infty^k)$ [47] to the ion energy levels and, finally, we modify the Saha–Boltzmann expression for the line emissivity of an ingredient element [47]:

$$\ln\left(\frac{I_1}{g_1}\frac{\lambda_1}{A_1}\right)^* = \ln\left(\frac{I_1}{g_1}\frac{\lambda_1}{A_1}\right) - \ln\left(6.04 \times 10^{21} \times \frac{T^{\frac{3}{2}}}{n_e}\right). \tag{1}$$

Now, we can make plots similar to Boltzmann plots for each species such as atomic as well as ionic using Equation (1). The accurate determination of electron temperature depends on ionic and atomic lines availability having large differences in upper-level excitation energies. Here, the average electron temperature was achieved from the Saha–Boltzmann-plots of Ca (I), and Ca (II) emission lines. The Saha–Boltzmann-plot achieved from sample-(α), the measured data-points were observed to be less dispersed ($R^2 \geq 0.98$) and the maximum of the Ca emission lines with a linear-trend as shown in Figure 3. The estimated temperature was 9000 ± 500 K.
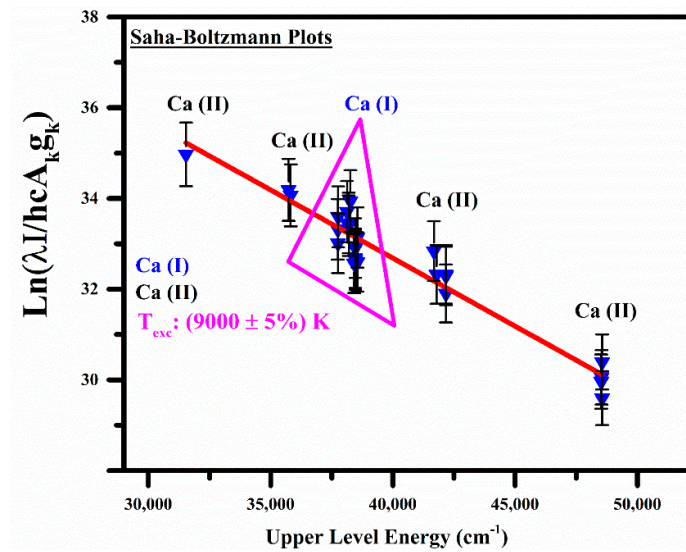

Figure 3. Saha–Boltzmann plots using the well-isolated Ca (I) and Ca (II) spectral lines.

3.3. Electron Plasma Number Density

To estimate the electron-number-density, the hydrogen line-profile was used and a well-isolated Stark broadened line profile of carbon belongs to the emission spectrum of the *P. harmala* seed sample-(α). The estimated number density using the full-width-at-half-area (FWHA) of a hydrogen (H_α) spectral-line emits at 656.3 nm wavelength is depicted in Figure 4a. The measured line profile data (blue color) and black dotted lines (vertical) indicate the FWHA produces as (0.643 ± 0.5) nm. A simple relation for measurement of electron-density using H_α-line is taken from Gigosos et al. [48] and Sherbini et al. [49].

$$\omega_{FWHA} = 5.49\text{\AA} \times \left(\frac{N_e}{10^{17}\text{cm}^{-3}}\right)^{0.67965} \tag{2}$$

Here, ω_{FWHA} represents the full-width-at-half-area and N_e denotes the number density. The ω_{FWHA} parameter is computed through the relation, $\omega_{FWHA} = \delta\omega_2 - \delta\omega_1$. The plasma density calculated using Equation (2) is $(1.26 \pm 0.5) \times 10^{17}$cm^{-3}. The full-width-at-half-maxima, $\Delta\lambda_{1/2}$ (FWHM) of C spectral-line was estimated using Voigt-fitting-line-profile by considering the 0.06 ± 0.01 nm instrumental-width, the Stark-width (ω_s) and 0.005 nm the Doppler-width. The Stark-width relation versus FWHM and plasma-electron-density is shown as follows [49]:

$$N_e(cm^{-3}) = \frac{\frac{\Delta\lambda_1(FWHM)}{2}}{2\omega_s(\lambda,T_{exc})} \times 10^{16}. \tag{3}$$

Here, ω_s represents the parameter of Stark-broadened, N_e shows the plasma-electron-density and T_{exc} shows the excitation-temperature. The Stark-broadened-line-profile of the C I emission line at 247.86 nm due to 2p3s $^1P_1 \rightarrow$ 2p^2 $^1S_0$ transition is shown in Figure 4b. The experimentally measured data-points (blue-circles) and Voigt fitting profile (the solid-orange-line) gives the FWHM (0.743 ± 0.5) nm. The Stark-broadened-parameter (the 0.0361 nm taken from literature [50]), the electron plasma density N_e is approximated as $(1.03 \pm 0.5) \times 10^{17}$ cm^{-3}. An excellent agreement can be found among densities calculated using Stark-Broadened spectral-line-profile of C I at corresponding wavelength 247.8 nm and the hydrogen-H$_\alpha$ emits at wavelength 656.3 nm. Besides, an average calculated num-ber-densities $(1.15 \pm 0.5) \times 10^{17}$ cm^{-3} was used to estimate the quantification of *P. harmala* samples with CF-LIBS.
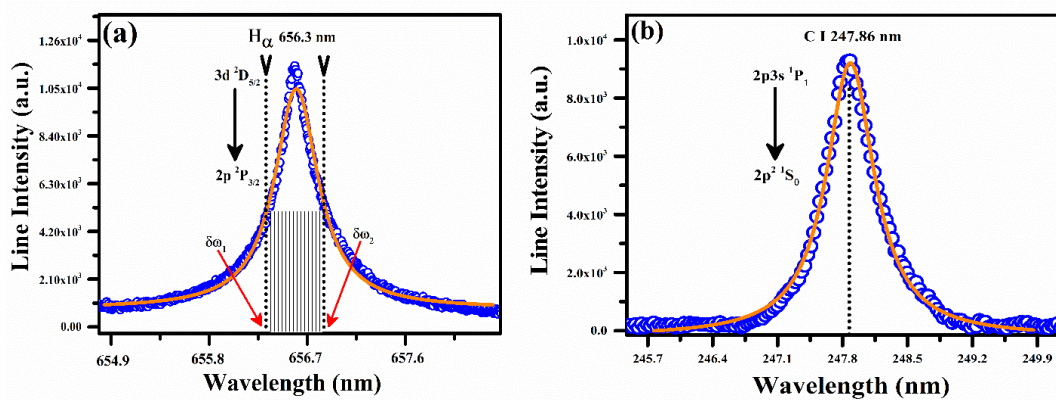

Figure 4. (**a**) H$_\alpha$ spectral line; (**b**) Stark-broadened-line-profile of C-I spectral line emits at wave-length 247.86 nm.

The estimated uncertainty in the electron number densities appears due to the uncer-tainties in the FWHM from the fitting procedure, from the instrumental-width, and star-broadened parameter. A criterion proposed by McWhirter— $N_e(\text{cm}^{-3}) \geq 1.6 \times 10^{12}\sqrt{(T_{\text{exc}}}(\Delta E_{(eV)})^3$ [51]—is necessary to satisfy LTE conditions in plasma, where T_{exc} is the excitation-temperature in kelvin (K) and ΔE represents the transition energy in elec-tron volt (eV). The calculated N_e value was ~ 1×10^{15} cm^{-3}, which is less than the N_e value estimated from relations (2) and (3). This shows that the plasma satisfies the condition of LTE. The plasma condition of LTE has also been established by measuring the diffusion-length criterion for an inhomogeneous-plasma [52]. As per following condition, the char-acteristic variation length "d" is much larger than the diffusion-length ($10\lambda < d$). In this work, the diffusion length has been calculated by using the neutral carbon emission line (C I). The diffusion length was calculated to be $\lambda \sim 1.7 \times 10^{-2}$ mm. This is less relative to characteristic variation plasma length, which is typically a few mm, ensuring the plasma is very near to the LTE. Since, the condition of optically-thin and in LTE plasma has been confirmed; hence, the measured plasma-parameters can be used to estimate elemental composition of elements via the CF-LIBS method.

3.4. Laser Irradiance (GW/cm²) and Spatial (mm) Dependence of Plasma Parameters

In this section, we studied variation in plasma-parameters versus laser irradiance and distance (mm) between the plasma plume and lens. We optimized experimental condi-tions such as 80 mJ fixed laser energy. A distance of 3 mm from the plasma-plume to the light collecting lens was kept perpendicular to laser beam and the target sample was fixed on a rotating stage having a rotation speed of ~12 rpm to ensure fresh surface for each laser pulse shot. Figure 5a shows the varying trend of electron density and excitation tem-perature versus laser irradiance covering the range from 0 to 20 GWcm^{-2} at laser wave-

length 532 nm. The solid (red-color) curve is showing the power law fitted pattern in electron density and excitation temperature data points. The measured electron temperature increases from 8300 to 8900 K. The electron temperature described by Milan and Laserna [53] at 10.6 GW/cm² using a 532 nm laser shows a reasonable agreement with the present work. Likewise, the electron density versus the laser-irradiance ranges from 0 to 20 GW/cm² shows a rising curve from 1.2×10^{17} to 1.45×10^{17} cm⁻³ at 532 nm. Figure 5b shows the spatial varying trend of excitation temperature and electron density. The power law fitting on the experimentally measured data points at 532 nm laser wavelength is depicted in Figure. 5 (solid-red-line). The excitation temperature reduces from 9000 to 8000 K. The excitation temperature close to the target is high and reduces with rising distance from the target-material. The higher temperature near the sample occurs due to higher plasma growth and cooling rates as well. Likewise, the electron density spatial distribution demonstrated a similar decaying trend as in excitation temperature. The electron density versus distance (0.5 to 3 mm) reduced from 1.7×10^{17} to 1.1×10^{17} cm⁻³.
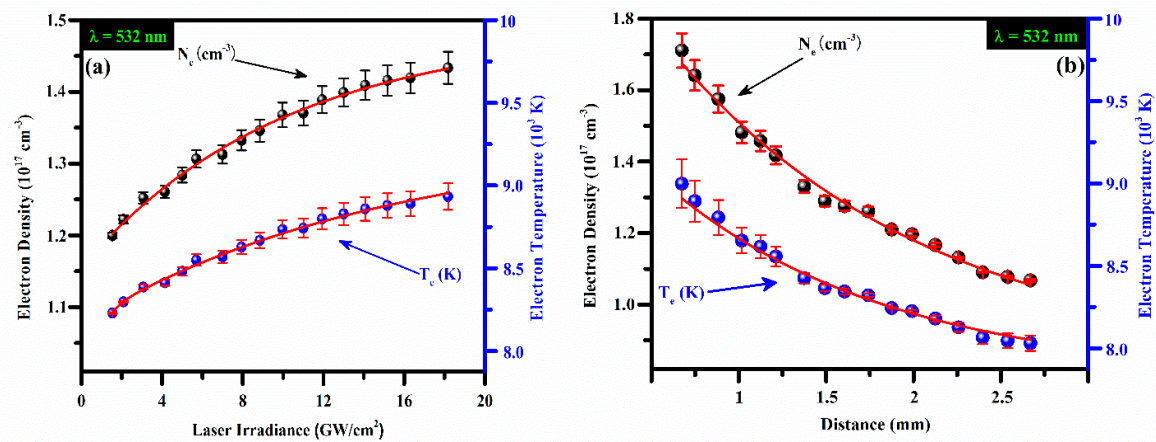

Figure 5. (**a**) The electron-temperature as well as electron number density of the plasma in a sample-(α) versus laser-irradiance ranges from 0 - 20 GW/cm² at 532 nm; (**b**) spatial varying behavior of the electron density and excitation plasma temperature in a sample-(α).

3.5. Quantitative Analysis Using CF-LIBS

The chemical-composition of seed sample-(α) was estimated using CF-LIBS technique. Ciucci et al. [54] described the detailed procedure for CF-LIBS to calculate the composition. In brief, it is established on the characterization of laser-induced plasma using a time-integrated spectrum through the excitation-temperature determination, and electron-density. For the CF-LIBS approach, the following conditions must be fulfilled.

a. Stoichiometric-laser induced ablation;
b. Local thermodynamical equilibrium (LTE);
c. Temporal and spatial homogeneity;
d. Optically thin lines.

Having established the above-mentioned conditions, we have calculated the chemical composition of the seed samples-(α, β, γ, and Δ). To find chemical composition of neutral-atoms ($C_{S(I)}$) in LIBS plasma of seed samples, the Boltzmann equation was utilized [54,55]:

$$F C_{S(I)} = I_{ki} \frac{P^{\gamma}(T)}{A_{ki} g_k} \exp\left[\frac{E_k}{k_B T}\right] \qquad (4)$$

Whereas, factor (*F*) represents the constant-for-constant-efficiency of system, $C_{S(I)}$ shows the neutral atom concentration, $P^{\gamma}(T)$ indicates the partition-function which depends on temperature, I_{ki} shows the measured spectral line intensity, g_k indicates the upper level

statistical weight of chosen transition, $A_{ki}(s^{-1})$ represents the transition probability of spectral transition which was taken from the NIST database, E_k (eV) is the energy of the upper-level, T is the measured electron temperature (eV), and k_B shows the Boltzmann constant. The composition of the ionized-species ($C_{S(II)}$) was achieved using Saha–Boltzmann-equation utilizing the neutral and corresponding ionized species [54].

$$N_e \frac{C_{S(II)}}{C_{S(I)}} = 6.04 \times 10^{21} \sqrt[3]{T_{eV}} \frac{U_{\alpha,\gamma+1}}{U_{\alpha,\gamma}} exp[-\frac{E_{\alpha,\gamma}}{k_B T}] \qquad (5)$$

Here, $E_{\alpha,\gamma}$ (eV) represents the α-element's ionization energy, N_e (cm^{-3}) indicates the electron-density, $C_{S(II)}$ is concentration of ionized species, $U_{\alpha,\gamma}$ and $U_{\alpha,\gamma+1}$ are partition-functions of lower charge-state (γ) and upper-charge-state ($\gamma+1$), respectively. The total composition of an ingredient element S is calculated using the relation [34, 55]:

$$C_S^\mu = C_{S(I)}^\mu + C_{S(II)}^\mu. \qquad (6)$$

The calculated average elemental chemical composition for major, minor, and trace ingredients is presented in Table 2 along with the standard deviation (SD). The chemical composition for major and minor ingredients is given as wt.%, while the composition of the trace elements is provided in micrograms per gram (μg/g). To calculate the relative errors in the composition, we calculated the SD of each element's composition exist in the target sample. The results obtained using CF-LIBS represents that C, Mg, and Ca are found as major ingredients, while K, Fe, Sr, Li, Na, and Si, are detected as minor ingredient elements. However, it is worth mentioning that Cu, Pb, and Zn are determined as traces in μg/g. Zn is detected only in the sample-(β, γ, and Δ) due to the doping of Zn in these samples as presented in Table 1. The results corresponding to the Zn composition in the doped samples show reasonable agreement. After determining the composition of ingredients, the next task is to classify the various *P. harmala* samples.

Table 2. Estimated average elemental composition of major (wt.%), minor (wt.%), and traces (μg/g) by CF-LIBS along with SD.

Element Chemical Composition (μg/g) ± SD			
	Sample-(α)	**Sample-(β)**	**Sample-(γ)**	**Sample-(Δ)**
Li (%)	2.87 ± 0.03	3.26 ± 0.01	2.18 ± 0.02	2.67 ± 0.05
C (%)	36.64 ± 0.16	34.81 ± 0.02	37.57 ± 0.17	36.55 ± 0.13
Na (%)	2.33 ± 0.02	2.57 ± 0.01	2.89 ± 0.03	3.92 ± 0.09
Mg (%)	24.09 ± 0.22	25.31 ± 0.03	23.31 ± 0.15	24.27 ± 0.18
Cu (μg/g)	8.07 ± 0.02	7.18 ± 0.01	9.44 ± 0.07	8.44 ± 0.02
Si (%)	3.72 ± 0.04	1.08 ± 0.01	2.98 ± 0.03	2.48 ± 0.08
K (%)	7.17 ± 0.17	6.91 ± 0.04	5.86 ± 0.11	6.63 ± 0.18
Ca (%)	19.03 ± 0.19	18.69 ± 0.06	17.75 ± 0.18	17.35 ± 0.07
Pb (μg/g)	1.10 ± 0.09	1.80 ± 0.04	1.73 ± 0.11	1.16 ± 0.15
Fe (%)	2.83 ± 0.02	1.42 ± 0.02	2.59 ± 0.03	1.79 ± 0.05
Sr (%)	1.14 ± 0.03	4.06 ± 0.05	4.32 ± 0.04	3.72 ± 0.03
Zn (μg/g)		48.6 ± 1.81	61.9 ± 1.74	76.5 ± 1.79

3.6. Principal Component Analysis

LIBS coupled with chemometrics methods offers a robust methodology to identify and classify various materials. PCA is a machine learning tool applied to data having high-ranked dimensions. The PCA test suppressed the dataset to significantly low dimensions from high-ranking dimensions correlated variables known as principal components (PCs). PCs are classified in descending order of the incorporated variance; PC1 includes the largest variance, and so on. PCA reduces the high dimensions using a scoring matrix [38,56] and is further used for the classification of the sample. The 10 *P. harmala* samples

averaged spectra within spectral-region varies from wavelength 220–720 nm are listed in Figure 6. The different spectral resemblances were noticed from the recorded LIBS spectra (three spectra's) of the doped samples. The 10 emission spectra were chosen as an average of 5 spectrum belongs to each sample. Two significant parameters such as eigenvalues and score plots are created using the PCA technique.
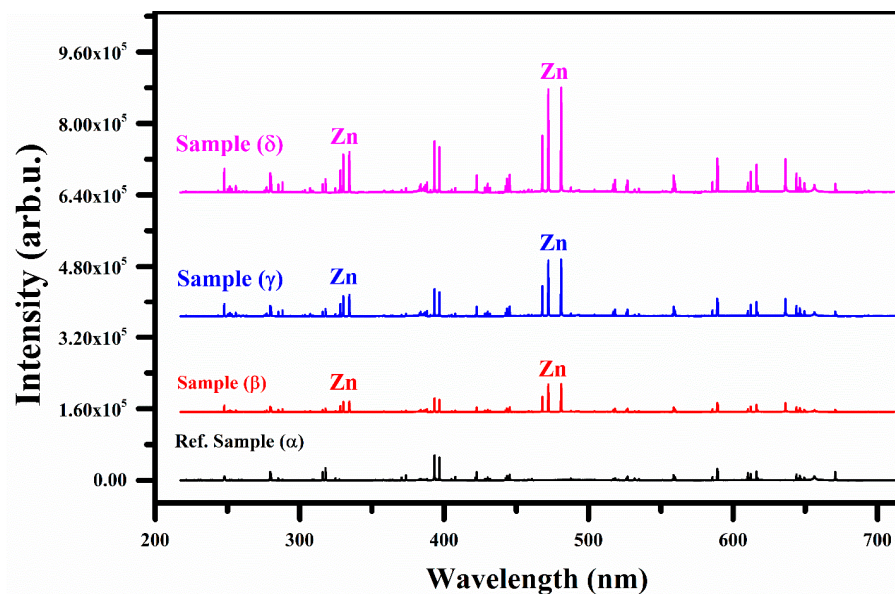

Figure 6. Average LIBS spectrum of the 3 doped *P. harmala* samples-(β, γ, and Δ) and one reference un-doped sample-(α).

Here, we employed PCA on the LIBS-spectra of 10 *P. harmala* samples having four classes namely; α, β, γ, and Δ. Three PCs calculated from the eigenvalues of the score matrix describe 87.6%, 4.6%, and 2.5% of variance for PC1, PC2, and PC3 respectively. The total-variance of the initial averaged LIBS spectral-data covered by the 3 PCS is ~94.7%. In Figure 7, the scree plot describes the variance covered by each PC from the LIBS spectral data set. The scree plot also recommends the essential PCs regard for classification purposes. The eigenvalues corresponding to the various PCs are plotted along the y-axis, showing 4 effective PCs having a maximum variance of the LIBS data. These four efficient PCs are enough to apply for the data discriminability; however, we only consider three PCs for the study of data clustering because three dimensions can be visualized at a time. Moreover, those spectral lines with significantly high SNR were selected to sketch the 3D-cluster-plot. We chose the line intensity of Ca (II), Zn (I), as well as C (I) at 393.4 nm, 481.05 nm, and 247.9 nm wavelengths, respectively. The 3D-cluster-plot was drawn with limited input-variables for discrimination of 4 *P. harmala* samples, as shown in Figure 8. The four isolated clusters, show various well-separated *P. harmala* samples including Ca, C, and Zn spectral lines. Hence, the spectral measurements of the three chosen elements Zn, C, and Ca present in the *P. harmala* samples show that these spectral lines can be suitable for the discrimination of plant samples.
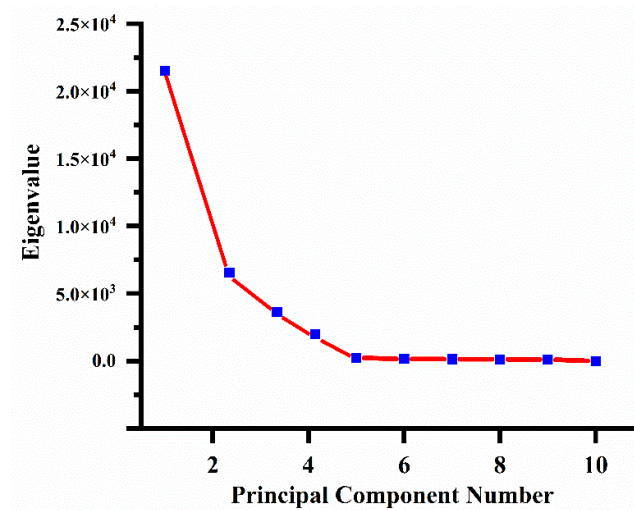
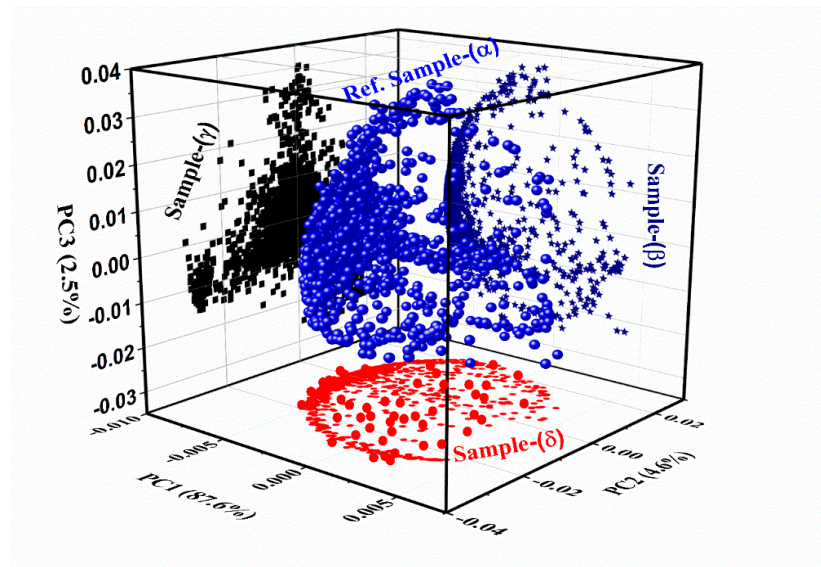**Figure 7.** Scree plot of the PCA analysis using averaged LIBS data.

Figure 8. Clustering of the various *P. harmala* samples from the PCA scatter plot.

3.7. Quantitative Analysis Using X-ray Fluorescence

X-ray-fluorescence (XRF) is a non-distractive analytical tool used to detect both major and minor ingredient elements up to ppm-level ranging from sodium (Na) (as a light element) to uranium (U) (as a heavy element) in various material samples such as liquid, solid, powder, and thin-film. This technique requires minimal sample preparation and gives rapid analysis. In this study, we used X-ray fluorescence, JSX-3202-M system worked at 5 to 50 kV varies from 0.01 - 1.0 mA with a power resolution of 150 eV at 6.0 keV for the elemental study of the seed samples.

In this work, all seed samples of *P. harmala* were analyzed using XRF for the determination of the chemical composition of the ingredient elements. The spectrum of the *P. harmala* seed sample-(α) is presented in Figure 9 showing the existence of Al, Mg, Si, Sr, Ca, K, Mn, Fe, Cu, Pb, Zr, and Ru. Furthermore, light elements including Li, Na, and C were not identified by XRF due to their detection limitations.
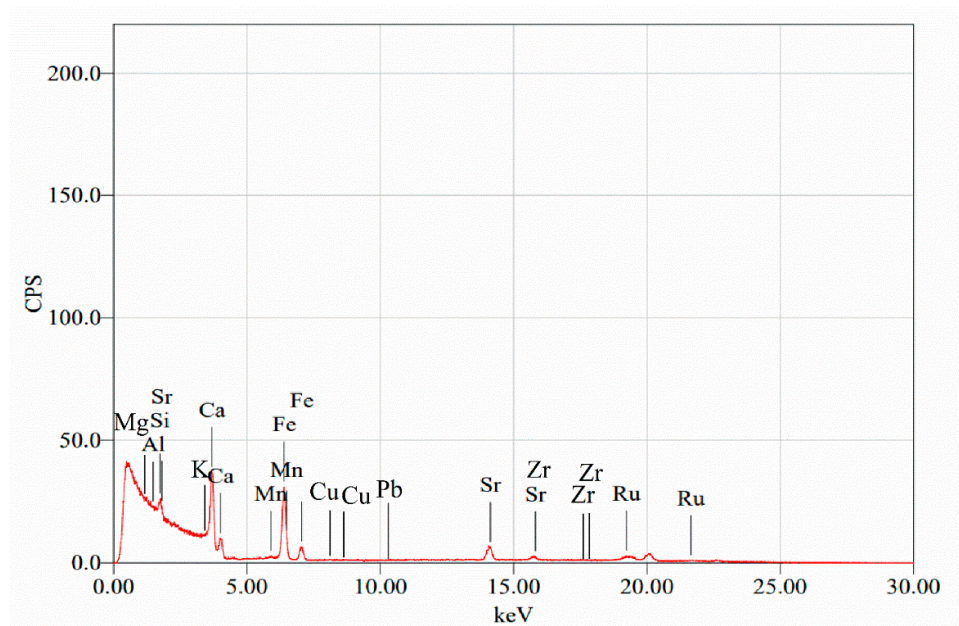
Figure 9. Elemental analysis of *P. harmala* seed sample-(α) using X-ray fluorescence spectroscopy.

3.8. Quantitative Analysis Using SEM-EDX

The surface morphology of the *P. harmala* seeds before and after doping of the pure zinc (μg/g), as well as the chemical composition, were investigated using the energy-dispersive X-ray (EDX) and SEM. The X-rays radiations released from the sample's surface were identified via a Si (Li) detector (30 mm^2). An Oxford-Instruments X-MAX-N-20 EDX-instrument connected with a SEM functioned at 30 keV was utilized to evaluate chemical composition of all seed samples. A spectrum of the *P. harmala* seed sample-(α) is presented in Figure 10a, showing the existence of Mg, Al, Na, Si, Sr, K, Ca, Rb, Cu, Pb, and Fe. The elements, Ca, Fe, Mg, and Cu are detected as major, and Na, Al, Si, Sr, K, and Rb are identified as minor ingredients. Furthermore, light elements including Li, and C were not detected by EDX due to its detection constraints. The morphology of all the seed samples was examined using SEM. In Figure 10b, we show an SEM micro-image of the surface of the seeds pallet with 4 μm high resolution showing the surface morphology of the *P. harmala* seed sample-(α). Prominent various grains correspond to different elements. The calcium sulfate and silica grains are observed to show a sufficient amount of calcium (Ca) and silicon (Si) in the sample.

In Figure 11, we present the chemical composition comparison in μg/g of analytical techniques such as CF-LIBS, XRF, and EDX. Interestingly, Si, Mg, Ca, Fe, K, Pb, Cu, and Sr are successfully identified by all the analytical techniques; however, some trace elements present in the samples were only identified by individual techniques due to their detection constraints. For instance, different elements including Zr, Ru, and Mn were detected only by XRF; similarly, Li, and C by LIBS, and Rb were only detected by EDX due to the elemental homogeneity and detection limits. Therefore, in a particular range, results show that Mg, K, Si, Ca, Fe, and Cu are the major identified elements of the seed samples.
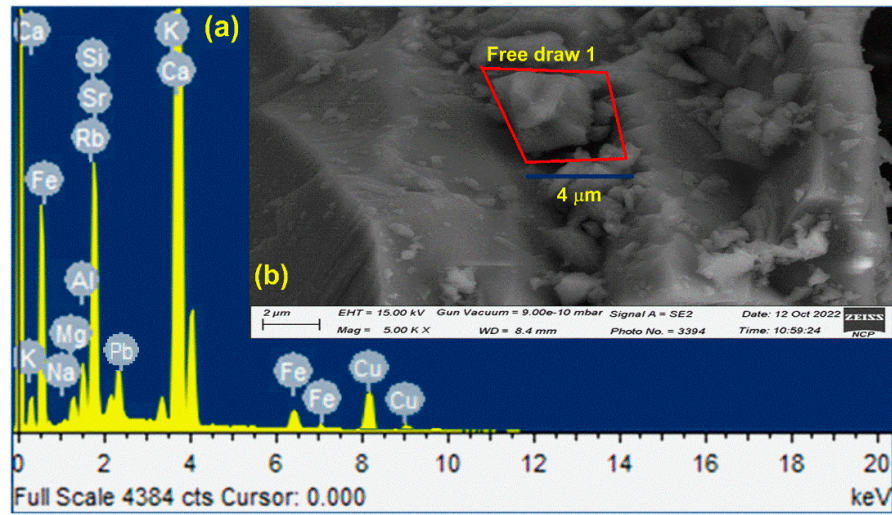
Figure 10. (**a**) EDX spectrum of the *P. harmala* seed sample-(α) at 30 keV; (**b**) SEM image of the *P. harmala* seed sample-(α) showing the surface morphology.
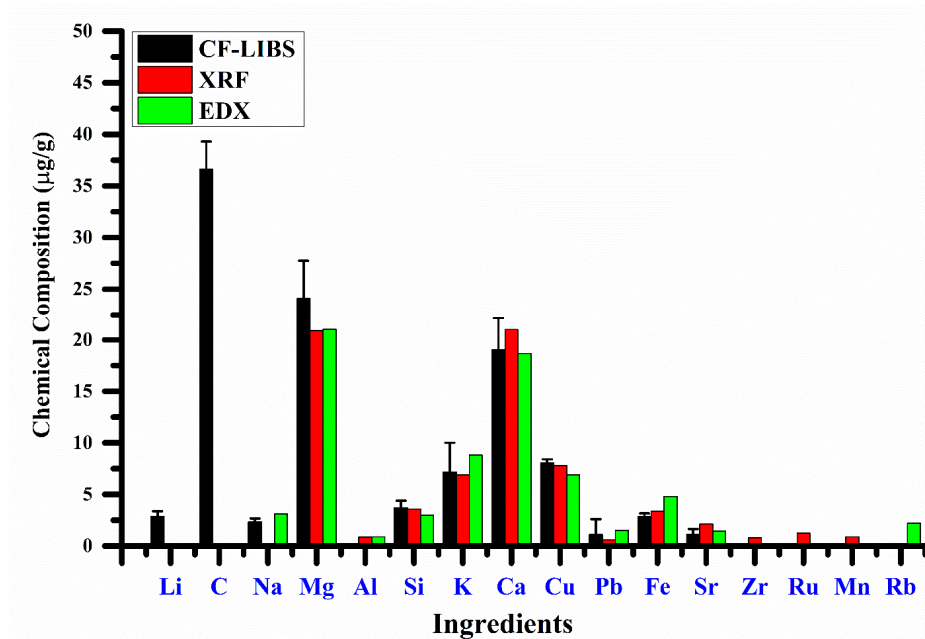

Figure 11. Chemical composition (μg/g) of the *P. harmala* seed sample-(α) using the CF-LIBS, XRF, and EDX.

4. Discussions

4.1. Limitations of the Techniques: EDX, XRF, and LIBS

EDX connected with SEM is usually employed for the qualitative analysis of a material. The EDX depth profile is normally around 5 microns and its detection limit is ~ 0.1 wt.%. Therefore, only those elements which are present in concentrations > 0.1% can be detected in the EDX analysis. The major elements with concentrations > 10% such as Si, Mg, K, Cu, Fe, and Ca are determined as major in all the analytical techniques as detected by EDX.

XRF was used here to analyze the same samples. The XRF technique has a depth profile of about 100 microns and the detection limit is ~ 0.01 wt.%. Therefore, the results again indicate that when the ingredient weight% in the sample >0.01% and the sample

size is greater than a few millimeters, then elements or constituents can be analyzed with better precision and would be quantified. The elements including Li, C and Na remained undetected due to the lower concentration of the element in the sample and also an XRF limitation. However, major elements with good concentration such as > 10% were detected successfully.

The LIBS qualitative/quantitative analysis of any sample, can be conducted without damaging the surface of the material. The LIBS depth profile is approximately hundreds of microns (~ 100 microns) with a detection limit of about 10–50 ppm. In the present study, the LIBS results are reliably showing a good detection limit. Interestingly, LIBS results are in reasonable agreement with that of the XRF and EDX, in the case of major-elements. However, EDX and XRF are quite deviating in the case of light elements such as Li, Na, and Mg due to their as-mentioned detection limits

5. Conclusions

In summary, the use of LIBS together with chemometric methods such as PCA was investigated to demonstrate the viability of the quick analysis of various *Peganum harmala* seed samples. The various ingredients, including minor, major, and trace elements including Na, H, Li, C, Mg, Ca, Si, Fe, K, Cu, Sr, and Pb, are identified in the seed samples using the LIBS technique. For quantitative study, the CF-LIBS technique subject to optically thin plasma and following LTE was implemented. The laser-stimulated plasma was precisely characterized using the plasma excitation-temperature including the electron number density. The elemental analysis using CF-LIBS showed that the C, Mg, and Ca are major, while Na, Li, Si, Fe, K, and Sr are minor elements exist in the samples. In particular, the results presented significant evidence of the relatively lower concentration (μg/g) of heavy-metals such as Pb and Cu, found in all the samples. Furthermore, PCA was applied to the spectral data achieved by using LIBS to differentiate different *Peganum harmala* seed samples. The LIBS spectral data variance covered by PC1, PC2, and PC3 was observed as ~94.7% of the entire variance. In addition, CF-LIBS results were incorporated with other analytical techniques such as XRF and EDX. The comparative study showed that the elements Mg, K, Si, Ca, Cu, and Fe are identified as major constituent of the *Peganum harmala* seed samples. Therefore, the results indicates that LIBS in combination with PCA, XRF, and EDX is a fast-growing tool for the identification and discrimination of seed samples compared with other techniques based on chemical methods.

Institutional Review Board Statement: Not applicable.

Informed Consent Statement: Not applicable.

Data Availability Statement: The data is available on request.

Conflicts of Interest: The authors declare no conflict of interest.

References

1. Yousefi, R.; Ghaffarifar, F.; Asl, A.D. The effect of Alkanna tincturia and Peganum harmala extracts on Leishmania major (MRHO/IR/75/ER) in vitro. *Iran. J. Parasitol.* **2009**, *4*, 40–47.
2. Khawar, K.M.; Ozel, C.A.; Balci, S.E.M.I.H.A.; Ozcan, S.E.B.A.H.A.T.T.I.N.; Arslan, O.R.H.A.N. Efficient shoot regeneration in Syrian rue (*Peganum harmala* L.) under in vitro Conditions. *Int. J. Agric. Biol* **2005**, *7*, 790–793.
3. Jinous, A.; Fereshteh, R. Chemistry, pharmacology and medicinal properties of Peganum harmala L. *Afr. J. Pharm. Pharmacol.* **2012**, *6*, 1573–1580.
4. Begum, Z.; Khan, T. An Allometric Growth Estimation of *Peganum harmala* L. Species Collected from Gilgit and Ghizir Districts of Gilgit-Baltistan, Pakistan.
5. Goel, N.; Singh, N.; Saini, R. Efficient in vitro multiplication of Syrian Rue (*Peganum harmala* L.) using 6-benzylaminopurine pre-conditioned seedling explants. *Nat. Sci.* **2009**, *7*, 129–134.
6. Mirzaie, M.; Nosratabadi, S.J.; Derakhshanfar, A.; Sharifi, I. Antileishmanial activity of Peganum harmala extract on the in vitro growth of Leishmania major promastigotes in comparison to a trivalent antimony drug. *Vet. Arh.* **2007**, *77*, 365–375.
7. ASGHARI, G.R.; Lockwood, G.B. Stereospecific Biotransformation of (±) Phenylethyl Propionate by Cell Cultures of *Peganum harmala* L. *Iran. Biomed. J.* **2002**, *6*, 43–46.
8. Zaker, F.; Oody, A.; Arjmand, A. A study on the antitumoral and differentiation effects of Peganum harmala derivatives in combination with ATRA on leukaemic cells. *Arch. Pharmacal Res.* **2007**, *30*, 844–849.
9. Singh, A.B.; Khaliq, T.; Chaturvedi, J.P.; Narender, T.; Srivastava, A.K. Anti-diabetic and anti-oxidative effects of 4-hydroxy-pipecolic acid in C57BL/KsJ-db/db mice. *Hum. Exp. Toxicol.* **2012**, *31*, 57–65.
10. Shahverdi, A.R.; Monsef-Esfahani, H.R.; Nickavar, B.; Bitarafan, L.; Khodaee, S.; Khoshakhlagh, N. Antimicrobial activity and main chemical composition of two smoke condensates from Peganum harmala seeds. *Z. Für Nat. C* **2005**, *60*, 707-710.
11. Darabpour, E.; Bavi, A.P.; Motamedi, H.; Nejad, S.M.S. Antibacterial activity of different parts of Peganum harmala L. growing in Iran against multi-drug resistant bacteria. *EXCLI J.* **2011**, *10*, 252.
12. Boulal, A.; Atabani, A.E.; Mohammed, M.N.; Khelafi, M.; Uguz, G.; Shobana, S.; Bokhari, A.; Kumar, G. Integrated valorization of Moringa oleifera and waste Phoenix dactylifera L. dates as potential feedstocks for biofuels production from Algerian Sahara: An experimental perspective. *Sahara Exp. Perspect. Biocatal. Agric. Biotechnol.* **2019**, *20*, 101234.
13. Herraiz, T.; González, D.; Ancín-Azpilicueta, C.; Arán, V.J.; Guillén, H. β-Carboline alkaloids in Peganum harmala and inhibition of human monoamine oxidase (MAO). *Food Chem. Toxicol.* **2010**, *48*, 839–845.
14. Mahmoudian, M.; Salehian, P.; Jalilpour, H. Toxicity of Peganum harmala: Review and a case report. *IJPT* **2002**, *1*, 1–4.
15. Anjum, S.; Bazai, Z.A.; Rizwan, S.; Benincasa, C.; Mehmood, K.; Siddique, N.; Shaheen, G.; Mehmood, Z.; Azam, M.; Sajjad, A. Elemental characterization of medicinal plants and soils from Hazarganji Chiltan National Park and nearby unprotected areas of Balochistan, Pakistan. *J. Oleo Sci.* **2019**, *68*, 443–461.
16. Ayazi, Z.; Banihashemi, M. Determination of trace amount of silver in water samples by flame atomic absorption after preconcentration by ZnO nano sorbent. *Sep. Sci. Technol.* **2016**, *51*, 585–593.
17. Alexander, D.; Ellerby, R.; Hernandez, A.; Wu, F.; Amarasiriwardena, D. Investigation of simultaneous adsorption properties of Cd, Cu, Pb and Zn by pristine rice husks using ICP-AES and LA-ICP-MS analysis. *Microchem. J.* **2017**, *135*, 129–139.
18. Jing, F.; Yang, Z.; Chen, X.; Liu, W.; Guo, B.; Lin, G.; Huang, R.; Liu, W. Potentially hazardous element accumulation in rice tissues and their availability in soil systems after biochar amendments. *J. Soils Sediments* **2019**, *19*, 2957–2970.
19. Shen, T.; Li, W.; Zhang, X.; Kong, W.; Liu, F.; Wang, W.; Peng, J. High-sensitivity determination of nutrient elements in panax notoginseng by laser-induced breakdown spectroscopy and chemometric methods. *Molecules* **2019**, *24*, 1525.
20. Dong, M.; Wei, L.; Lu, J.; Li, W.; Lu, S.; Li, S.; Liu, C.; Yoo, J.H. A comparative model combining carbon atomic and molecular emissions based on partial least squares and support vector regression correction for carbon analysis in coal using LIBS. *J. Anal. At. Spectrom.* **2019**, *34*, 480–488.
21. Sheta, S.; Afgan, M.S.; Hou, Z.; Yao, S.C.; Zhang, L.; Li, Z.; Wang, Z. Coal analysis by laser-induced breakdown spectroscopy: A tutorial review. *J. Anal. At. Spectrom.* **2019**, *34*, 1047–1082.
22. Xue, B.; Tian, Y.; Lu, Y.; Li, Y.; Zheng, R. Characteristics of the secondary breakdown of DP-LIBS in bulk water with different axial focusing arrangements and laser energies. *Spectrochim. Acta Part B At. Spectrosc.* **2019**, *151*, 20–25.
23. Meng, D.; Zhao, N.; Wang, Y.; Ma, M.; Fang, L.; Gu, Y.; Jia, Y.; Liu, J. On-line/on-site analysis of heavy metals in water and soils by laser induced breakdown spectroscopy. *Spectrochim. Acta Part B At. Spectrosc.* **2017**, *137*, 39–45.
24. Kumar Myakalwar, A.; Spegazzini, N.; Zhang, C.; Kumar Anubham, S.; Dasari, R.R.; Barman, I.; Kumar Gundawar, M. Less is more: Avoiding the LIBS dimensionality curse through judicious feature selection for explosive detection. *Sci. Rep.* **2015**, *5*, 13169.
25. Wang, Q.; Teng, G.; Li, C.; Zhao, Y.; Peng, Z. Identification and classification of explosives using semi-supervised learning and laser-induced breakdown spectroscopy. *J. Hazard. Mater.* **2019**, *369*, 423–429.
26. Singh, V.K.; Kumar, V.; Sharma, J. Importance of laser-induced breakdown spectroscopy for hard tissues (bone, teeth) and other calcified tissue materials. *Lasers Med. Sci.* **2015**, *30*, 1763–1778.
27. Andrade, D.F.; Pereira-Filho, E.R. Direct determination of contaminants and major and minor nutrients in solid fertilizers using laser-induced breakdown spectroscopy (LIBS). *J. Agric. Food Chem.* **2016**, *64*, 7890–7898.

28. Jiang, T.J.; Guo, Z.; Ma, M.J.; Fang, L.; Yang, M.; Li, S.S.; Liu, J.H.; Zhao, N.J.; Huang, X.J.; Liu, W.Q. Electrochemical laser induced breakdown spectroscopy for enhanced detection of Cd (II) without interference in rice on layer-by-layer assembly of graphene oxides. *Electrochim. Acta* **2016**, *216*, 188–195.

29. Peng, J.; He, Y.; Zhao, Z.; Jiang, J.; Zhou, F.; Liu, F.; Shen, T. Fast visualization of distribution of chromium in rice leaves by re-heating dual-pulse laser-induced breakdown spectroscopy and chemometric methods. *Environ. Pollut.* **2019**, *252*, 1125–1132.

30. Miziolek, A.W.; Palleschi, V.; Schechter, I. (Eds.) *Laser Induced Breakdown Spectroscopy*; Cambridge University Press: Cambridge, UK, 2006.

31. Cremers, D.A.; Radziemski, L.J. *Handbook of Laser-Induced Breakdown Spectroscopy*; John Wiley & Sons: Hoboken, NJ, USA, 2013.

32. Singh, J.P.; Thakur, S.N. *Laser-Induced Breakdown Spectroscopy*; Elsevier: Amsterdam, The Netherlands, 2007.

33. Tognoni, E.; Palleschi, V.; Corsi, M.; Cristoforetti, G.; Omenetto, N.; Gornushkin, I.; Smith, B.W.; Winefordner, J.D. From sample to signal in laser-induced breakdown spectroscopy: A complex route to quantitative analysis. In *Laser-Induced Breakdown Spectroscopy (LIBS) Fundamentals and Applications;* Cambridge Univ. Press: Cambridge, UK, 2006; pp. 122–170.

34. Hahn, D.W.; Omenetto, N. Laser-induced breakdown spectroscopy (LIBS), part I: Review of basic diagnostics and plasma–particle interactions: Still-challenging issues within the analytical plasma community. *Appl. Spectrosc.* **2010**, *64*, 335A–366A.

35. Hahn, D.W.; Omenetto, N. Laser-induced breakdown spectroscopy (LIBS), part II: Review of instrumental and methodological approaches to material analysis and applications to different fields. *Appl. Spectrosc.* **2012**, *66*, 347–419.

36. Guo, G.; Niu, G.; Shi, Q.; Lin, Q.; Tian, D.; Duan, Y. Multi-element quantitative analysis of soils by laser induced breakdown spectroscopy (LIBS) coupled with univariate and multivariate regression methods. *Anal. Methods* **2019**, *11*, 3006–3013.

37. Yao, M.; Rao, G.; Huang, L.; Liu, M.; Yang, H.; Chen, J.; Chen, T. Simultaneous analysis of Cr and Pb in contaminated pork by laser-induced breakdown spectroscopy. *Appl. Opt.* **2017**, *56*, 8148–8153.

38. Alrebdi, T.A.; Fayyaz, A.; Asghar, H.; Elaissi, S.; Maati, L.A.E. Laser Spectroscopic Characterization for the Rapid Detection of Nutrients along with CN Molecular Emission Band in Plant-Biochar. *Molecules* **2022**, *27*, 5048.

39. Alrebdi, T.A.; Fayyaz, A.; Asghar, H.; Zaman, A.; Asghar, M.; Alkallas, F.H.; Hussain, A.; Iqbal, J.; Khan, W. Quantification of Aluminum Gallium Arsenide (AlGaAs) Wafer Plasma Using Calibration-Free Laser-Induced Breakdown Spectroscopy (CF-LIBS). *Molecules* **2022**, *27*, 3754.

40. Iqbal, J.; Asghar, H.; Shah, S.K.H.; Naeem, M.; Abbasi, S.A.; Ali, R. Elemental analysis of sage (herb) using calibration-free laser-induced breakdown spectroscopy. *Appl. Opt.* **2020**, *59*, 4927–4932.

41. Fayyaz, A.; Liaqat, U.; Adeel Umar, Z.; Ahmed, R.; Aslam Baig, M. Elemental Analysis of Cement by Calibration-Free Laser Induced Breakdown Spectroscopy (CF-LIBS) and Comparison with Laser Ablation–Time-of-Flight–Mass Spectrometry (LA-TOF-MS), Energy Dispersive X-Ray Spectrometry (EDX), X-Ray Fluorescence Spectroscopy (XRF), and Proton Induced X-Ray Emission Spectrometry (PIXE). *Anal. Lett.* **2019**, *52*, 1951–1965.

42. Plemmons, D.H.; Parigger, C.; Lewis, J.W.; Hornkohl, J.O. Analysis of combined spectra of NH and N 2. *Appl. Opt.* **1998**, *37*, 2493–2498.

43. Liu, Y.; Gigant, L.; Baudelet, M.; Richardson, M. Correlation between laser-induced breakdown spectroscopy signal and moisture content. *Spectrochim. Acta Part B At. Spectrosc.* **2012**, *73*, 71–74.

44. Lucena, P.; Doña, A.; Tobaria, L.M.; Laserna, J.J. New challenges and insights in the detection and spectral identification of organic explosives by laser induced breakdown spectroscopy. *Spectrochim. Acta Part B At. Spectrosc.* **2011**, *66*, 12–20.

45. Alrebdi, T.A.; Fayyaz, A.; Ben Gouider Trabelsi, A.; Asghar, H.; Alkallas, F.H.; Alshehri, A.M. Vibrational Emission Study of the CN and C2 in Nylon and ZnO/Nylon Polymer Using Laser-Induced Breakdown Spectroscopy (LIBS). *Polymers* **2022**, *14*, 3686.

46. Mousavi, S.J.; Hemati Farsani, M.; Darbani, S.M.R.; Mousaviazar, A.; Soltanolkotabi, M.; Eslami Majd, A. CN and C2 vibrational spectra analysis in molecular LIBS of organic materials. *Appl. Phys. B* **2016**, *122*, 106.

47. Aguilera, J.A.; Aragón, C. Characterization of a laser-induced plasma by spatially resolved spectroscopy of neutral atom and ion emissions: Comparison of local and spatially integrated measurements. *Spectrochim. Acta Part B At. Spectrosc.* **2004**, *59*, 1861–1876.

48. Gigosos, M.A.; Gonzalez, M.A.; Cardenoso, V. Computer simulated Balmer-alpha,-beta and-gamma Stark line profiles for non-equilibrium plasmas diagnostics. *Spectrochim. Acta Part B At. Spectrosc.* **2003**, *58*, 1489–1504.

49. El Sherbini, A.M.; Hegazy, H.; El Sherbini, T.M. Measurement of electron density utilizing the Hα-line from laser produced plasma in air. *Spectrochim. Acta Part B At. Spectrosc.* **2006**, *61*, 532–539.

50. Griem, H.R. *Spectral Line Broadening by Plasmas*; Academic Press: New York, NY, USA; London, UK, 1974.

51. McWhirter, R.W.P. *Plasma Diagnostic Techniques*; Huddlestone, R.H., Leonard, S.L., Eds.; Academic: New York, NY, USA, 1965.

52. Cristoforetti, G.; De Giacomo, A.; Dell'Aglio, M.; Legnaioli, S.; Togoni, E.; Palleschi, V.; Omenetto, N. Local Thermodynamic Equilibrium in Laser-Induced Breakdown Spectroscopy: Beyond the McWhirter criterion Spectrochim. *Acta Part B* **2010**, *65*, 86–95.

53. Milan, M.; Laserna, J.J. Diagnostics of silicon plasmas produced by visible nanosecond laser ablation. *Spectrochim. Acta Part B At. Spectrosc.* **2001**, *56*, 275–288.

54. Ciucci, A.; Corsi, M.; Palleschi, V.; Rastelli, S.; Salvetti, A.; Tognoni, E. New procedure for quantitative elemental analysis by laser-induced plasma spectroscopy. *Appl. Spectrosc.* **1999**, *53*, 960–964.

55. Fayyaz, A.; Liaqat, U.; Yaqoob, K.; Ahmed, R.; Umar, Z.A.; Baig, M.A. Combination of laser-induced breakdown spectroscopy, and time–of–flight mass spectrometry for the quantification of CoCrFeNiMo high entropy alloys. *Spectrochim. Acta Part B At. Spectrosc.* **2022**, *198*, 106562.
56. Wang, J.; Liao, X.; Zheng, P.; Xue, S.; Peng, R. Classification of Chinese herbal medicine by laser-induced breakdown spectroscopy with principal component analysis and artificial neural network. *Anal. Lett.* **2018**, *51*, 575–586.